Control and power balancing of an off-grid wind turbine with co-located electrolyzer

Victor Timmers, Agustí Egea-Àlvarez, Aris Gkountaras, Lie Xu

***Abstract*—Co-locating electrolyzers and offshore wind can significantly reduce the cost of green hydrogen. However, without a grid connection, a new control paradigm is required for the electrolyzer to follow the variable power supplied by the wind turbine. Commercial electrolyzers have power ramp rate limitations, which can result in a mismatch between the wind turbine and electrolyzer power, leading to frequent shutdown and potentially unstable operation. This paper is the first to develop a control system for this off-grid operation with three mechanisms to dynamically balance the power, including energy storage, rotor inertia, and enhanced pitch control. The results show that a $6.8M supercapacitor is required with a power rating and capacity of approximately 6.7 MW and 8.5 kWh to enable the system to operate through 99% of the annual wind variation. If the electrolyzer ramp rates can be doubled, the same operating hours can be achieved using only control-based power balancing methods at the cost of a marginal reduction in energy production. If commercial electrolyzer ramp rates can be tripled, the system is able to operate without the need for any power balancing.**

***Index Terms*—Wind power generation, hydrogen, power generation control, energy storage, grid-forming control**

NOMENCLATURE

A. Symbols

A	Swept area [m^3]
C_p	Power coefficient
$i_{d,q}$	Direct- and quadrature-axis stator current [A]
K_{C_p}	Optimal MPPT gain
K_J	Inertia factor
$L_{d,q}$	Direct- and quadrature-axis inductance [H]
P_{el}	Electrolyzer power consumption [W]
P_m^*	Machine power reference from MPPT [W]
p	Number of pole pairs
R_s	Stator resistance [Ω]
P_{wt}	Wind turbine aerodynamic power input [W]
V_{DC}	DC link voltage [V]
v	Wind speed [m/s]
$v_{d,q}$	Direct- and quadrature-axis stator voltage [V]
β	Pitch angle [°]
ΔP	Power mismatch [W]
λ	Tip speed ratio
λ_m	Flux linkage [Wb]
ρ	air density
τ_m	Machine torque [Nm]
$\tau_{m,J}^*$	Inertia adjusted torque reference [Nm]
ω_e	Electrical rotational speed [rad/s]
ω_m	Machine rotational speed [rad/s]
ω_{nom}	Nominal rotor rotational speed [rad/s]
ω_r	Rotor rotational speed [rad/s]

B. Abbreviations

BoL	Beginning-of-life
BPF	Band-pass filter
EoL	End-of-life
ESCC	Electrolyzer-side converter control
ICC	Inner current control
J-V	Current density – voltage
LSCC	Line-side converter control
LUT	Look-up table
MSCC	Machine-side converter control
MPPT	Maximum power point tracking
MTPA	Maximum torque per ampere
PEM	Proton-exchange membrane
PLL	Phase-locked loop
PMSG	Permanent magnet synchronous generator
P-V	Power-voltage
PWM	Pulse-width modulation
VSC	Voltage source converter
VSM	Virtual synchronous machine
WT	Wind turbine

I. INTRODUCTION

Hydrogen has the potential to displace fossil fuels in sectors which are otherwise difficult to decarbonise, such as heavy industry, shipping, and aviation [1]. It also has the potential to be an alternative to batteries for large scale, long-term energy storage. Hydrogen is an energy carrier, and not an energy source, so its climate impact is entirely dependent on the method used to produce it. Currently, most of the world's hydrogen comes from natural gas, emitting CO_2 in the process. To avoid these emissions, the hydrogen needs to be produced using water electrolysis powered by renewable energy, so called green hydrogen [1].

There are several barriers to the widespread adoption of green hydrogen electrolysis. One of the main challenges is the relatively high cost of production [2]. In addition, electrolysis requires a steady supply of water and has a limited efficiency [3]. For green hydrogen specifically, the intermittency of renewable energy sources complicates the operation of hydrogen electrolyzers. These can have strict operating limits, such as

This work was supported in part by the UK Engineering and Physical Sciences Research Council (EPSRC) under Industrial Cooperative Award in Science and Engineering (ICASE) grant number EP/T517665/1, and in part by Siemens Gamesa Renewable Energy.

Victor Timmers, Agustí Egea-Àlvarez, and Lie Xu are with the Department of Electronic and Electrical Engineering, University of Strathclyde, Glasgow.

Aris Gkountaras is with Siemens Gamesa Renewable Energy, Germany.

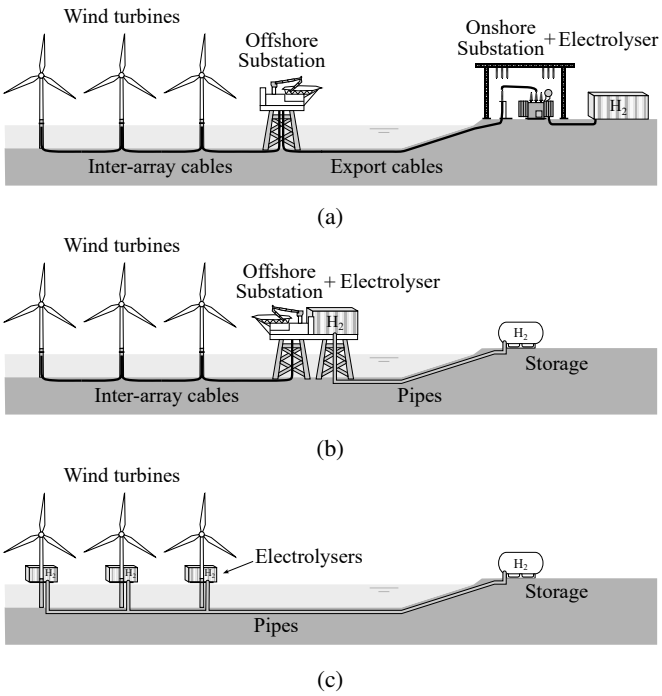

Fig. 1: Offshore wind-powered electrolysis configurations, (a) centralised onshore electrolyzer, (b) centralised offshore electrolyzer, (c) co-located electrolyzer

minimum load requirements, maximum power ramp-up and ramp-down rates, and long start-up and restart times [4].

Using offshore wind energy to produce green hydrogen offers the potential to overcome these barriers. The relatively high and consistent wind speeds found offshore result in less intermittency. The offshore location allows seawater to be used after desalination [5] and research into using seawater directly is ongoing [6].

There are three main configurations of offshore wind hydrogen production, illustrated in Fig. 1. These include a centralised electrolyzer located onshore powered by an offshore wind farm, a centralised electrolyzer located offshore, and decentralised electrolyzers co-located with individual wind turbines [5]. This study considers the third configuration.

Co-locating the electrolyzer with the wind turbine can result in significantly reduced electrical infrastructure costs [7]. These off-grid wind turbines would require no additional cables to connect to the power grid, instead using pipelines to transport the hydrogen, which can be 10 to 20 times cheaper to build [1] and can have a lifetime of 40 to 80 years [8]. This direct connection of wind turbine and electrolyzer also has the benefit of not requiring local grid reinforcements and the associated planning and construction costs [7].

Despite a significant increase over the last decade in the number of publications concerning hydrogen electrolyzers [9], much of the work on wind-hydrogen systems has focused on the economic aspects [10]–[12]. Very little research considers off-grid wind turbines directly connected to electrolyzers, and there are currently no studies on how such a system could be operated and controlled.

A. State of the art

Standalone wind-powered electrolysis is not a new idea [13], but the wind industry has only recently started commercial research and development. Commercial wind power hydrogen production projects are still in the early development stages, and either consist of small-scale onshore test facilities, such as the Brande Hydrogen project [14], or larger scale grid-connected projects, such as the Holland Hydrogen I project [15]. There has been no research yet on the operation and control of an off-grid, commercial-scale offshore wind turbine with co-located electrolyser.

Academic research into the concept is also limited to small-scale systems that focus on hydrogen output over long time-scales without significant consideration of the system dynamics. In [16], a 10 kW vertical axis wind turbine directly connected to a proton-exhange membrane (PEM) electrolyzer was simulated. The electrolyzer performance characteristics were determined based on a set of experiments on a 56 W electrolyzer cell. The electrolyzer was connected to the wind turbine through a full bridge diode rectifier followed by a buck converter. The hydrogen production was then calculated based on measured wind speed data from an observation facility. Despite using realistic wind speed and electrolyzer data, this study did not use commercial-scale wind turbines or electrolyzers. It also only included steady-state operation and did not investigate or account for the wind turbine or electrolyzer dynamics.

Research by [17] investigated the integration of an alkaline electrolyzer with a 6.8 kWp photovoltaic solar array and a 6 kW wind turbine in a stand-alone system. The study assessed the system efficiency and energy balance over the course of one year. One of the main findings is that the limitations of commercial electrolyzers, such as the lower operating limit and the number of stops permitted by manufacturers, is a main challenge in this type of systems. The authors proposed running the electrolyzer below the minimum operating limit for short durations or using battery storage to minimise the number of stops and increase the system efficiency. However, this study did not investigate the power conversion process in detail, instead simply taking into account conversion losses. The energy balancing performed in this study only included the minimum operating limit and did not account for electrolyzer ramp rates.

A study by [18] looked into maximum power point tracking (MPPT) control strategies for a micro wind turbine rated at 250 W connected to an electrolyzer stack. The authors considered how to increase the system efficiency by employing more complex MPPT strategies than the conventional hill climb and verified this experimentally. However, the study was limited to the MPPT algorithm for a DC/DC converter and did not include the control of any other wind turbine elements. It also did not consider commercial-scale power ratings or any of the commercial electrolyzer limitations.

B. Contributions

This study is the first to investigate the operation and control of a commercial-scale standalone wind turbine with

an integrated electrolyzer, including the dynamic balancing of power between the wind turbine and electrolyzer in such an off-grid system.

Currently, no research exists on how a standalone wind turbine can be controlled to successfully integrate the electrolyzer without any grid connection. This study develops a comprehensive control strategy, which includes grid-forming control of the line-side converter, as well as grid-following control of the generator converter and electrolyzer converter.

In addition, this is the first paper to demonstrate that off-grid wind turbines electrolyzer systems cannot operate by simply using their existing control structures, due to the different dynamic responses of the wind turbine and electrolyzer. Existing studies only consider steady-state operation of electrolyzers, whereas this paper takes into account the electrolyzer ramp-rate limitations.

This study is the first to quantify the potential power and energy mismatch between the wind turbine and electrolyzer due to their differing dynamic response, based on realistic wind speed variation.

In addition, this study proposes and assesses the viability of three novel mechanisms to balance the power between the input wind and the electrolyzer, including energy storage, rotor inertia, and enhanced pitch control. This study also demonstrates how the wind turbine control can be enhanced to incorporate these balancing strategies.

Finally, this study is the first to quantify the trade-offs of each of the balancing mechanisms, including financial costs of the energy storage system, and the efficiency costs of the rotor inertia and enhanced pitch control strategies.

This paper is organised as follows: in section II, the challenges of operating a ramp-rate limited electrolyzer without grid connection are discussed, in section III the modelling methodology and converter control structures are introduced. In section IV, section V, and section VI the implementation of three power balancing strategies are described, including energy storage, rotor inertia and pitch control. Section VII sets out the conclusions.

II. Challenges of off-grid operation

Practically all commercial electrolyzers are connected to the grid, where they can operate continuously at rated power or adjust their loading to provide grid support services [19], [20]. However, when electrolyzers are supplied by a single wind turbine without a grid connection, their loading will vary continuously depending on the available power in the wind. As a result, the electrolyzer limitations such as its minimum loading and maximum power ramp rate become much more significant.

A. Electrolyzer limitations

Despite the near-instantaneous reaction of the electrolyzer cells to changes in current [21], the balance of plant will have a more limited ramp-up and ramp-down rate to ensure safe operation [22]. In the literature, estimates for allowable power ramp rates vary wildly, with studies suggesting ramp rates ranging from 0.01 pu/s [23] to 2.5 pu/s [24]. The size and design of the electrolyzer will have a large impact on this ramp rate. Therefore, this study uses current commercially available PEM electrolyzers specifically targeted towards wind turbine applications as a basis. These typically have ramp rate limitations of 0.1 pu/s [25]. In addition, many commercial electrolyzers use a modular structure where multiple stacks are connected in parallel to achieve high power ratings. A higher number of stacks reduces the impact of the minimum loading, since the individual stacks can be switched off when the generated power falls below the minimum load level. However, a higher number of stacks results in stricter ramp rate limitations, since any stacks not in operation must start up before being able to accept changes in loading.

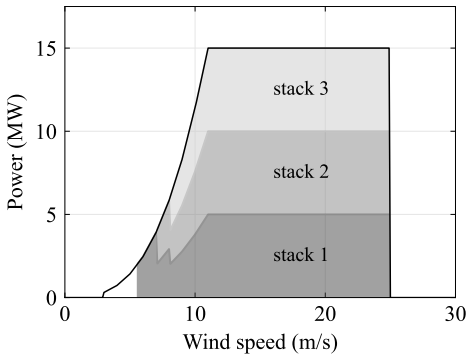

Fig. 2: Power consumption per stack for varying wind speeds

For this study, a 15 MW PEM electrolyzer was considered, consisting of three independent stacks of 5 MW each. Since the stacks are more efficient at lower operating points, they are set to equally share the power from the wind turbine. New stacks are added as soon as the power increases to allow all to operate at the minimum load [26]. This is illustrated in Fig. 2.

B. Power mismatch

When the wind speed changes rapidly, the power output from the wind turbine may exceed the ramp rate limitation of the electrolyzer, resulting in a power mismatch. An example of the impact of a rapid decrease in wind speed illustrated in Fig. 3a. The electrolyzer ramp-down limitation will cause the power demanded to be higher than the power available in the wind. The mismatch between power results in a slowdown of the wind turbine. From the wind turbine aerodynamic curve, it can be seen that a decrease in rotational speed results in a further decrease in power, as shown in Fig. 4a. The result is an unstable feedback loop where the slow down of the wind turbine causes the mismatch between electrolyzer and wind turbine to increase, further slowing the turbine down until it completely stops and the electrolyzer has to be disconnected.

Depending on the electrolyzer specifications, frequent shutdown may result in significant hydrogen production losses due to the long restart time, and frequent shutdown may also affect the degradation and lifetime of the system [22]. To prevent this from happening, a mechanism must be introduced to balance the wind turbine and electrolyzer power. This allows the wind turbine to maintain its speed long enough for the electrolyzer demand to catch up. Once it does, the wind turbine can recover

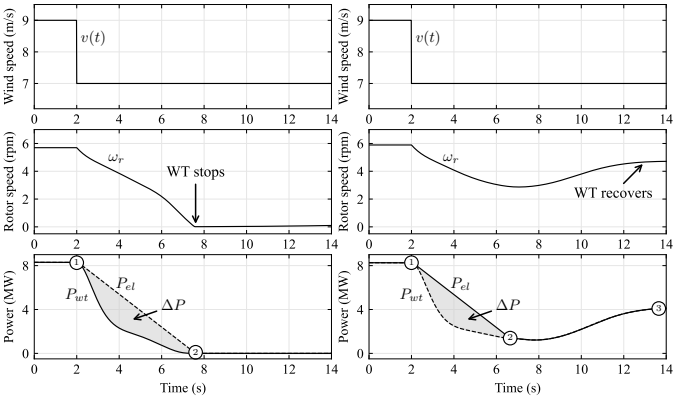

(a) (b)

Fig. 3: Power mismatch between wind turbine and electrolyzer following a rapid reduction in wind speed, (a) without power balancing, (b) with power balancing

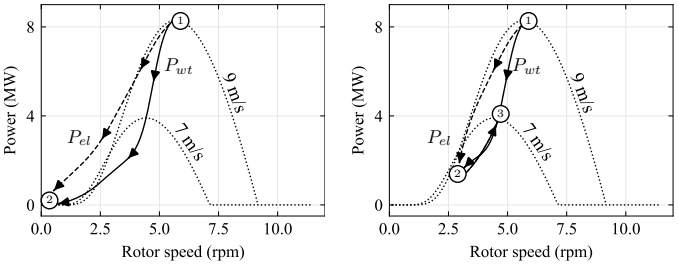

(a) (b)

Fig. 4: Wind turbine aerodynamic power curve showing the changing operating point following a wind speed reduction, (a) without power balancing, (b) with power balancing

and continue operating at the new wind speed. This is shown in Fig. 3b and Fig. 4b.

If the wind speed increases, the wind power will be higher than the electrolyzer demand, resulting in a potentially dangerous speed-up of the turbine or an unacceptable rise in the system voltage. Traditional wind turbines regularly experience a similar scenario at high wind speeds where the wind power exceeds the rated power of the wind turbine. For this, pitch control can be used to feather the blades to reduce the power captured by the wind turbine. The same pitching mechanism can in theory be used to reduce the wind turbine power output when it exceeds the electrolyzer ramp-up limitation.

However, the electrolyzer ramp rate can interfere with the stable operation of this pitch control. Since the electrolyzer ramp rate limits how fast the wind turbine power can change, this can cause the pitch controller to overcompensate. Any overshoot of the pitch can decrease the available power in the wind faster than the electrolyzer ramp rate, which has the potential to result in the same unstable feedback loop encountered for a rapid wind speed decrease.

It is therefore necessary to design a wind control system that allows for off-grid operation, including the incorporation of mechanisms that can temporarily provide additional power to balance the wind turbine output and electrolyzer demand.

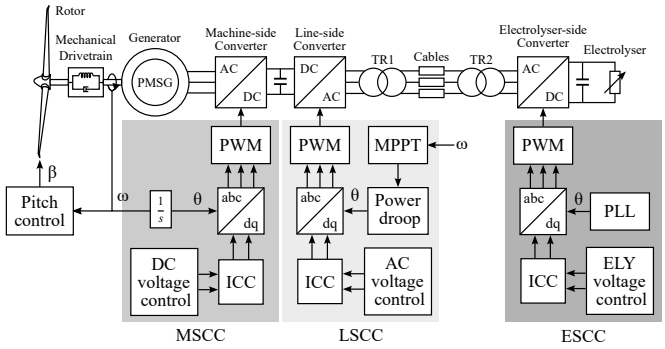

Fig. 5: Overview of the complete model with high level control structure for the machine-side converter control (MSCC), line-side converter control (LSCC) and electrolyzer-side converter control (ESCC)

III. Modelling and Control

The system under study is an off-grid commercial wind turbine directly connected to an electrolyzer. The model was built using MATLAB/Simulink. The wind turbine is a generic type 4 configuration, with a nominal power rating of 15 MW. The wind turbine uses a low voltage permanent magnet synchronous generator (PMSG) and fully-rated back-to-back power converter. The power converters use a two-level voltage source converter (VSC) topology. A transformer is used to step up the converter output to 66 kV before the power is transmitted by three-phase cables down the tower. At the base of the tower, a second transformer reduces the voltage and a VSC rectifies the voltage before delivering the power to the electrolyzer.

An overview of the complete model with the high level control structures is shown in Fig. 5. The following sections describe each of the components and their control in detail.

A. Rotor

The wind turbine rotor model takes the wind speed, pitch angle and rotational speed as inputs, calculates the tip speed, power coefficient C_p, power extracted from the wind and outputs the resulting torque. The modelling approach taken is based on [27], [28]. The aerodynamic power input of the wind turbine can be calculated using the equation

$$P_{wt} = \frac{1}{2} C_p(\lambda, \beta) \rho A v^3 \tag{1}$$

where ρ is the air density, A is the swept area, v is the wind speed, and $C_p(\lambda, \beta)$ is the nonlinear power coefficient, which is dependent on the tip speed ratio, λ, and the blade pitch angle, β. It can be calculated using a lookup table or parametric equations [28].

B. Standard pitch control

The standard pitch control system aims to keep the wind turbine rotational speed at or below the nominal speed. The wind turbine pitch controller and actuator were modelled using the approach taken in [29], [30]. The control block diagram

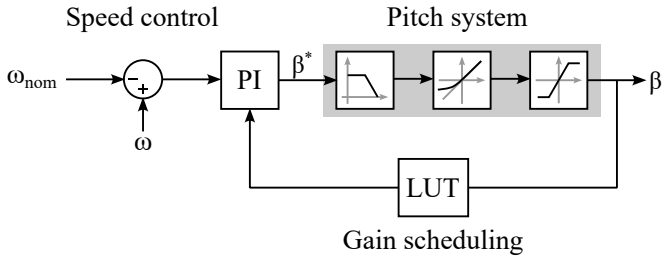

Fig. 6: Control block diagram for the standard pitch controller and acutator

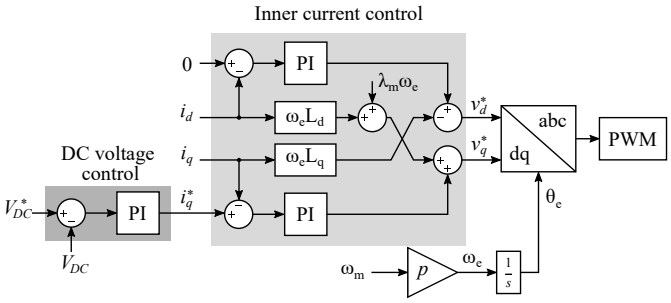

Fig. 7: Control block diagrams for the machine-side converter

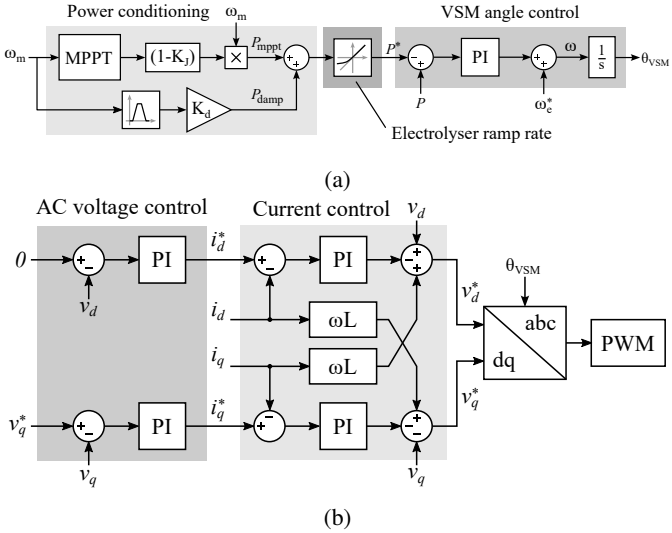

Fig. 8: Control block diagrams for the line-side converter, (a) power conditioning and VSM control, (b) voltage and current control

is shown in Fig. 6. The standard pitch control system uses a proportional-integral (PI) controller to generate a pitch angle set point based on the difference of the nominal and the measured rotor speed.

Due to the highly nonlinear aerodynamic torque characteristic as a function of the pitch angle, the PI controller gains are adjusted using gain scheduling based on a look-up table (LUT) [29]. The pitch actuator system itself is represented by a low pass filter with a time constant of 0.3 seconds, a rate of change limiter with a 10°/s limit, and a saturation block with limits between 0° and 90°.

C. Drive-train and generator

The wind turbine rotor is connected to the generator via the mechanical drive-train. The conventional method of representing the response of this system is using a multiple mass model. A two-mass model was used as it can capture the dynamics that affect stability, whereas higher-order models are typically used to study mechanical details such as fatigue of the drive-train [31]. The two-mass model was implemented in the form of a state-space model following the procedure set out in [32].

The generator is a PMSG and is modelled following the approach used by [32]. The torque developed by the PMSG can be calculated using

$$\tau_m = \frac{3}{2} p\big(\lambda_m i_q + (L_d - L_q) i_q i_d\big) \tag{2}$$

Where p is the number of pole pairs, $i_{d,q}$ are the stator currents, λ_m is the flux linkage, and $L_{d,q}$ are the stator inductances. The subscripts d and q denote the direct and quadrature axes of the rotating reference frame, respectively.

D. Machine-side converter and control

The purpose of the machine-side converter is to generate the stator voltages of the PMSG to obtain the desired stator currents. Several control structures are possible to set the current references for type-4 wind turbines, depending on the task division of the converters [33]. For the off-grid wind turbine, the DC link voltage is controlled by the machine-side converter.

The control consists of a classic PI based outer loop voltage controller, followed by an inner current controller, with a maximum torque per ampere (MTPA) configuration. This is illustrated in Fig. 7 and described in more detail in [29].

The converter itself is modelled using the average converter model to reduce the computational requirements of the simulation. This consists of a controlled voltage source connected to the AC side and a controlled current source connected to the DC side [34]. The voltage set points from the current control loop can then be used to directly control the voltage sources.

E. Line-side converter and control

In grid-connected wind turbines, the line-side converter uses grid-following control with a phase-locked loop (PLL) to synchronise with the grid. However, in the case of the off-grid wind turbine, there is no grid to synchronise to. Instead, the line-side converter uses grid-forming control to generate its own voltage and frequency.

The grid-forming control system for the line-side converter is illustrated in Fig. 8a. The control strategy used is PI-based virtual synchronous machine (VSM) control, which emulates the traditional swing equation of synchronous machines.

The VSM control can be implemented by using a PI controller which compares the active power reference and measured power [35].

The active power reference is set by the power conditioning control, which consists of the MPPT power calculation, driv-

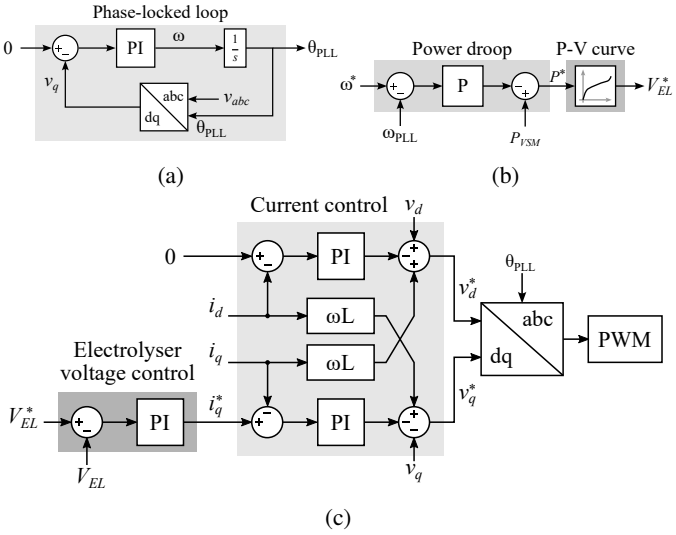

Fig. 9: Control block diagrams for the electrolyzer-side converter, (a) phase-locked loop, (b) power droop voltage set-point calculation, (c) electrolyzer voltage and current control

etrain active damping and electrolyzer ramp rate limitation. The MPPT power is calculated using

$$P_m^* = K_{Cp}\omega_m^3 \tag{3}$$

where K_{Cp} is a parameter based on the wind turbine characteristics to obtain the maximum power [28]

In regular wind turbine operation, the MPPT provides inherent drivetrain damping due to its dependence on rotor speed [36]. However, in the proposed system, the power set point cannot always change fast enough due to the limited electrolyzer ramp rate. As a result, the system requires active damping to prevent unwanted speed oscillations.

The active damping is based on [36] and consists of a band-pass filter (BPF) followed by a gain. The resulting damping power is added to the MPPT set point.

In addition to generating the electrical angle, the line-side converter is also tasked with controlling the AC voltage of the tower cables and transformers. This is achieved through the use of a cascaded voltage control and current control, illustrated in Fig. 8b, which have a similar structure to those used in the machine-side converter.

F. Electrolyzer-side converter and control

The purpose of the electrolyzer-side converter is to rectify and control the electrolyzer voltage, transferring the remaining power after losses in the transformers and tower cables.

The electrical angle used for the dq transformations is obtained by employing a phase-locked loop (PLL) to synchronise with the line-side converter frequency. The block diagram for the PLL is shown in Fig. 9a.

The electrolyzer voltage needs to be controlled to match the power remaining in the line after losses in the transformers and cables. This is done through a power droop control, as shown in Fig. 9b. The PLL angular velocity is compared with the nominal angular velocity with a P-controller. The output is

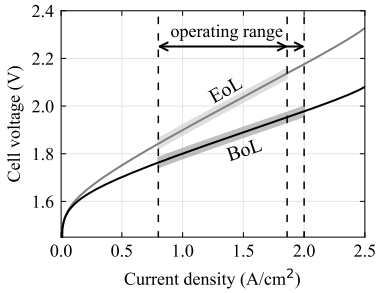

Fig. 10: Electrolyzer cell J-V characteristic

subtracted from the line-side converter power to provide the remaining power set point. The electrolyzer voltage is selected based on the electrolyzer P-V curve, which is dependent on the electrolyzer characteristics, which is discussed in more detail in section III-G. The electrolyzer voltage can then be controlled using the same cascaded controller structure as for the line-side converter, shown in Fig. 9c.

G. Electrolyzer

The electrolyzer is modelled using a controlled current sink. The current value is calculated based on the applied voltage using the electrolyzer cell performance, fed through a low pass filter to represent the electrolyzer cell dynamics.

The cell performance is characterised by the J-V curve, which represents the relationship between the current density and the cell voltage. It can be modelled using parametric equations, such as those proposed by [37], given by

$$V_{cell} = V_{oc} + V_{act} + V_\Omega + V_{con} \tag{4}$$

where V_{oc} is the open circuit voltage, which is calculated with

$$V_{oc} = \frac{\Delta G}{2F} + \frac{RT}{2F}\log\left(\frac{p_{H_2}\sqrt{p_{O_2}}}{p_{H_2O}}\right) \tag{5}$$

where ΔG is the change in Gibb's free energy, F is the Faraday constant, R is the ideal gas constant, T is the cell temperature, and p_{H_2}, p_{O_2}, and p_{H_2O} are the partial pressures of hydrogen, oxygen, and water, respectively. The activation overvoltage, V_{act} is calculated using

$$V_{act} = \frac{RT}{2F\alpha}\text{arcsinh}\left(\frac{J}{2J_0}\right) \tag{6}$$

where α is the charge transfer coefficient, J is the cell current density, and J_0 is the exchange current density. The ohmic overvoltage due to the internal resistance of the cell is given by

$$V_\Omega = rJ \tag{7}$$

where r is the total resistance of the electrolyzer in $\Omega\cdot\text{cm}^2$. Finally, the concentration overvoltage, V_{con} is represented by

$$V_{con} = \frac{RT}{2F}\ln\left(\frac{J_L}{J_L - J}\right) \tag{8}$$

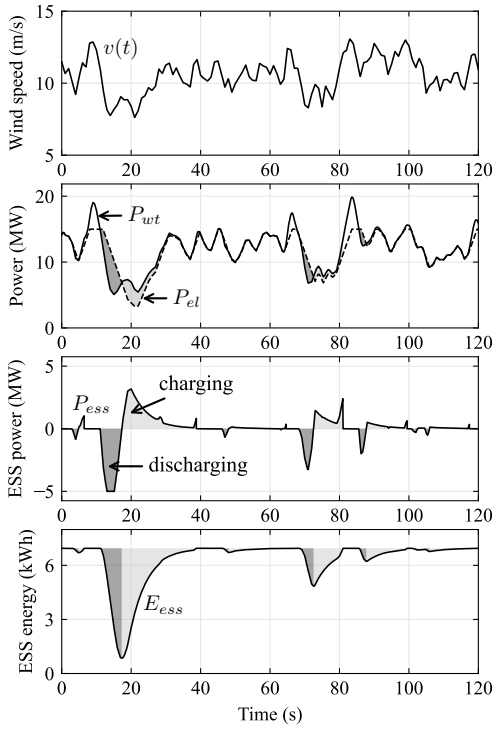

Fig. 11: Time domain results showing a two-minute window of realistic wind speeds, the power mismatch, and the resulting charging and discharging of the energy system storage

where J_L is the limiting current density. The parameters for the equation were selected to approximate the performance of a typical commercial electrolyzer for this application.

As the electrolyzer ages, its performance deteriorates due to degradation. The electrolyzer is considered to be at its end-of-life (EoL) when the required voltage is 10% higher compared to its beginning-of-life (BoL). The resulting J-V curves are shown in Fig. 10.

IV. Power balancing using energy storage

A. Mechanism

The most straightforward way of making up the difference in power between the wind turbine and the electrolyzer is by introducing energy storage. This is connected to the DC-link of the back-to-back converter through a dedicated DC/DC converter. The storage-side converter now takes on the control objective of managing the DC link voltage. This allows the machine-side converter control to set the wind turbine power based solely on the optimal torque set by the unconstrained MPPT. Any difference in power between the generator and electrolyzer is now compensated by the energy storage. The power set-point for the line-side converter VSM can be temporarily reduced to charge the energy system storage.

Using energy storage to balance the power has the advantage of enabling the wind turbine to operate at its maximum power point continuously. However, the main drawback of this balancing method is the high capital cost of the storage and the interfacing converter.

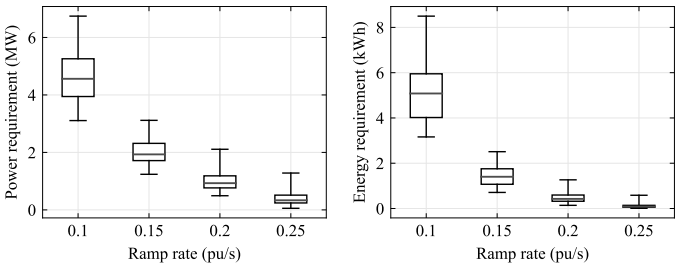

Fig. 12: Maximum hourly balancing requirements for varying electrolyzer ramp rates, (a) power requirements (b) energy requirements

B. Energy storage sizing

To calculate the size and cost of the energy storage, the difference between the power generated by the wind turbine and the ramp-rate limited electrolyzer power demand must be calculated. This power difference will be highly dependent on the wind conditions in which the turbine operates. Therefore, to estimate the requirements, first realistic wind speeds need to be modelled.

To simulate a realistic wind speed profile, the approach set out in [38] was adopted, which combines short-term wind turbulence with medium- and long-term wind variations based on the van der Hoven spectrum [39].

The stochastic nature of the wind speed and delay between wind speed and wind turbine power output mean that the likely power and energy mismatch between the wind turbine and the electrolyzer cannot be calculated analytically.

A Monte Carlo approach was therefore taken. One hundred hour-long realistic wind speed profiles were simulated with varying initial conditions. The available power input to the wind turbine was calculated using (1). The wind turbine dynamics were simplified to reduce the computational cost of the hour-long simulations by using low pass filters to determine the wind turbine rotational speed and pitch blade angle. The filter constants were adjusted to provide a good match with the more complex dynamic model described in section III.

Any rapid decrease in wind turbine power will require additional power to match the electrolyzer ramp-down rate. For the base case, the electrolyzer ramp-rate limitation is assumed to be 0.1 pu/s and is dependent on the number of stacks in operation, taken from Fig. 2. The maximum power difference can then be calculated and this can be integrated to obtain the energy mismatch. A 25% safety margin was added to the energy requirement to account for multiple wind speed decreases in rapid succession.

Fig. 11 shows example time-domain results for a challenging two-minute window in one of the hour-long realistic wind speed simulations. This case shows that a 5 MW, 7 kWh energy storage system allows the wind turbine to continue operating through the worst-case power mismatch event.

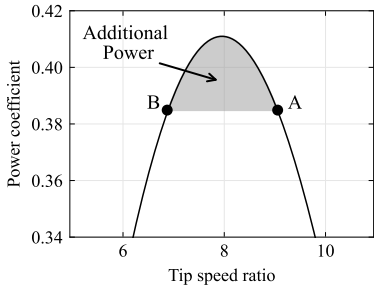

Fig. 13: Additional power available from rotor inertia

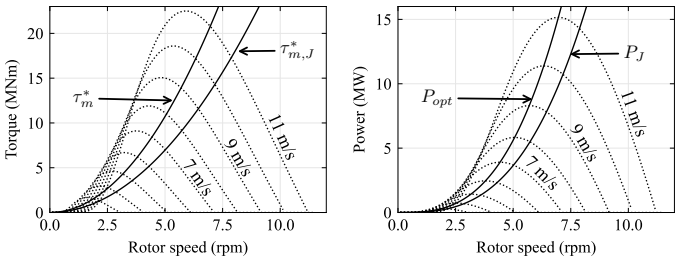

(a) (b)

Fig. 14: Comparison of standard and updated MPPT operating curves, (a) generator torque, (b) resulting aerodynamic power

C. Results

The results for all 100 wind speed scenarios for varying electrolyzer ramp rates are shown in Fig. 12.

The results show that for the electrolyzer to continuously operate during 99% of the hours below rated wind speed, the balancing power and energy requirements are 6.7 MW and 8.5 kWh, respectively. The most suited energy storage technology to fulfil these requirements would be a supercapacitor, due to its rapid dynamic response and high power delivery for a duration from seconds to minutes. The projected cost of supercapacitors in 2025 is $835/kW [40]. This corresponds to an additional capital cost of $5.6M. The associated DC/DC converter would add another $1.2M [41], which would significantly increase the cost of hydrogen production.

The electrolyzer ramp rate is the main factor determining these power and energy requirements. In the base case, an electrolyzer ramp rate of 0.1 pu/s is used. Further realistic wind speed simulations were performed for the nominal wind speed to determine how the requirements change with higher allowable ramp rates. The results of this investigation are shown in Fig. 12. The results show that doubling the allowable ramp rate to 0.2 pu/s reduces the 99% survival power requirements by 70% to 2.1 MW and the corresponding energy requirements by 85% to 1.3 kWh. A supercapacitor of this size with its associated converter is projected to cost approximately $2.1M.

If the electrolyzer has a ramp rate of 0.3 pu/s or above, power balancing is no longer required since the electrolyzer can follow the wind turbine power output without any significant mismatch.

V. Power balancing using rotor inertia

A. Mechanism

It is possible to use the wind turbine rotor to store energy in the form of inertia. This can then be used when the generator power drops faster than the electrolyzer ramp-down rate. When the wind turbine is operating at the peak of the power coefficient curve, any changes in the wind turbine speed will result in a reduction in power.

However, if the operating speed is increased, it is possible to gain additional power that can be used to match the electrolyzer ramp rate. This process is illustrated in Fig. 13. The wind turbine operates at point A, which is faster than its optimal operating point. When the wind speed drops and the generator power reduces faster than the electrolyzer ramp-down rate, the wind turbine will slow down, moving left along the Cp curve. This results in an increase in available power, until point B is reached. In addition, the higher operating speed means there is additional time for the electrolyzer power demand to catch up to the new output power before the wind turbine stops.

The advantage of using the rotor inertia is that, unlike the energy storage solution, no additional expensive components are required. However, the wind turbine will need to operate at a higher rotational speed than it was designed for, which may lead to reliability issues. The wind turbine will also produce less energy during regular operation due to its suboptimal operating speed.

For the wind turbine to operate at this higher rotational speed, the MPPT algorithm needs to be updated. This can be done by adding an inertia factor to the torque calculation, resulting in

$$\tau^*_{m,J} = (1 - K_J) K_{Cp} \omega_m^2 \tag{9}$$

where $\tau^*_{m,J}$ is the updated generator torque reference and K_J is the inertia factor that reserves part of the torque for rotor energy storage. Fig. 14a shows how the new MPPT and torque influences rotor speed, and Fig. 14b shows the resulting wind turbine power. It can be seen from the figure that the new MPPT torque reference results in a higher rotor speed but a small decrease in wind turbine power output.

B. Results

To estimate the required inertia factor, the new MPPT algorithm was tested on all 100 realistic wind speed scenarios from section IV-B. The inertia factor was adjusted iteratively until the wind turbine managed to stay operational through the event. The time domain results for the most challenging wind speed reduction are shown in Fig. 15. This shows that at inertia factors of less than 0.5, the wind turbine stalls and comes to a standstill, whereas at inertia factors of 0.5 and above, the wind turbine can survive the wind speed reduction.

The results for the remaining inertia balancing tests are shown in Fig. 16. For the base case 0.1 pu/s ramp rate, to enable the wind turbine to operate continuously through 99% of the wind speed variation, the required inertia factor is 0.45. In steady-state operation, this suboptimal torque setting results in a 10.6% loss in energy production for wind speeds below nominal. The wind turbine rotational speed also increases by 17.8%. This is a significant increase, which could potentially

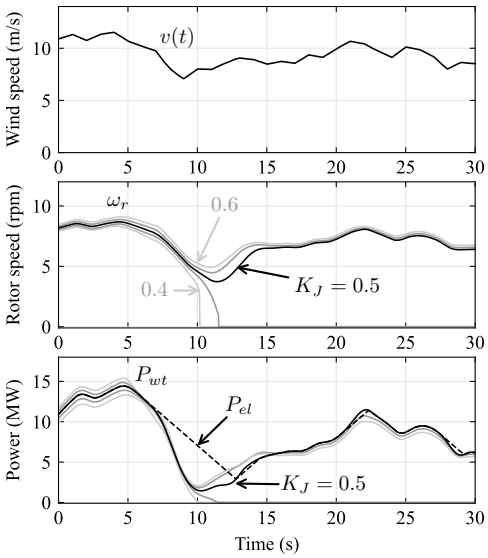

Fig. 15: Time domain results for the inertia balancing mechanism showing the impact of the inertia factor during the most challenging wind speed reduction

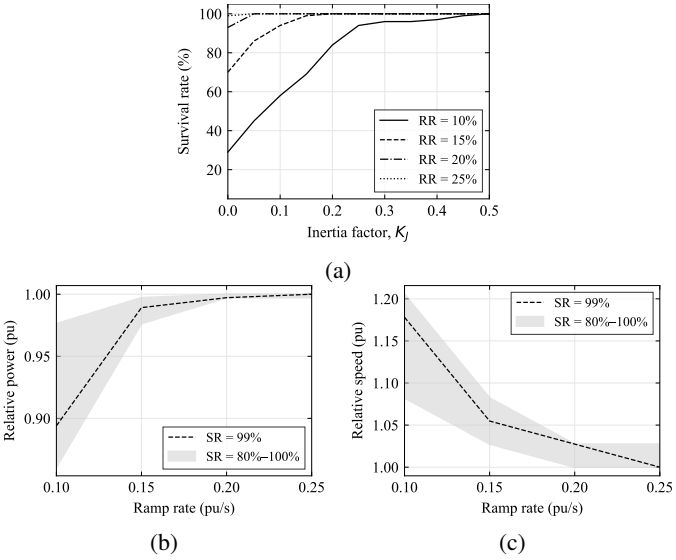

Fig. 16: Inertia balancing results for varying electrolyzer ramp rates (RR), (a) hourly survival rate (SR) by inertia factor, (b) impact on power production by SR, (c) impact on rotor speed by SR

result in a reduced wind turbine lifetime due to the additional stress on the rotor. It may also require a redesign of several control systems to prevent unwanted excitations.

If the electrolyzer ramp rate can be increased, the required inertia factor can be reduced while still allowing the wind turbine to continue operating. For example, doubling the allowable electrolyzer ramp rate to 0.2 pu/s was found to require an inertia factor of 0.05 for a 99% survival rate. This corresponds to a much more acceptable 0.3% energy loss and 2.7% rotational speed increase.

VI. Power balancing using pitch control

A. Mechanism

Pitching the wind turbine blades is already used in wind turbines to limit the speed and power during high wind speeds. It is therefore well suited to balancing the wind turbine and electrolyzer power for rapid wind speed increases. Increasing the pitch angle reduces the coefficient of performance and therefore the power extracted from the wind.

The main drawback with using pitch control for power balancing is that it cannot easily accommodate the electrolyzer ramp-down limitation. When the wind turbine operates below rated speed, the pitch angle is set to zero for maximum power extraction. In this case, a reduction in wind speed cannot be mitigated as any pitching will only further reduce the power.

A potential solution to this is to operate the wind turbine with a non-zero pitch below rated power. This allows the wind turbine to increase its power production temporarily during a wind speed reduction by decreasing the pitch angle. Operating at this non-zero pitch will alter the power coefficient curve, which means that the MPPT algorithm will need to be updated to determine the new operating speed. There are two options for updating the MPPT. The first is to set the MPPT to maintain the existing tip speed ratio, resulting in the same rotational speed of the wind turbine. The second option combines the inertia balancing method and non-zero pitch methods by adjusting the MPPT to find the new optimal rotational speed for the non-zero pitch curve.

The process for the first option is illustrated in Fig. 17a using an example non-zero pitch of 1°. During regular operation, the wind turbine will operate with a 1° pitch at its original tip speed ratio, indicated by point A, which is below its optimal point. When the wind speed and associated power drops faster than the electrolyzer ramp-down rate, the wind turbine will pitch the blades to zero, increasing the power production to the peak of the 0° curve, at point B. The power demand from the electrolyzer exceeds the provided power from the wind, resulting in a slow-down of the wind turbine. As the wind turbine slows down, the tip speed ratio decreases, and the operating point moves down the 0° curve. At point C, the power provided by the wind turbine is equal to the original power production at 1°, which denotes the limit of the additional power available. This option results in slightly lower power extraction from the wind compared to using a higher tip speed ratio. However, it has the advantage of not requiring the wind turbine to operate above its design speed.

The alternative is to use the new optimal tip speed ratio for non-zero pitch operation. This process is illustrated in Fig. 17b for an example non-zero pitch of 1°. During regular operation, the wind turbine will operate at the peak of the Cp curve for 1°, denoted by point A. When the wind speed drops, the blades are pitched to 0°, moving the operating point to the 0° curve, reaching point B. As the wind turbine slows down due to the electrolyzer power demands, the operating point moves down the 0° curve, with point C indicating the limits of the additional power. This option results in the highest efficiency operation. However, similar to using the rotor inertia balancing, in this case the wind turbine will need to operate at a higher rotational

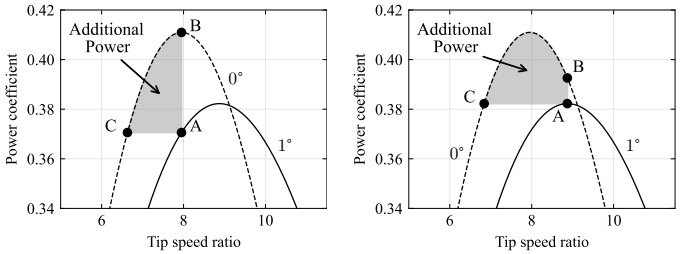

Fig. 17: Additional power available from non-zero pitch operation with MPPT set to (a) maintain existing tip speed ratio, (b) find the new optimal tip speed ratio

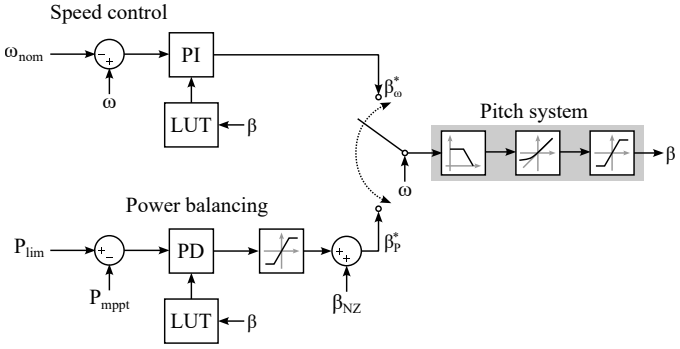

Fig. 18: Control block diagram for the enhanced pitch controller with power balancing capability

speed than it was designed for, which may lead to reliability issues.

The pitch controller can be enhanced to allow for power balancing below rated wind speed. This is done by adding a proportional-derivative (PD) controller to provide the pitch angle based on the difference between the aerodynamic power and the ramp-limited power demand, as shown in Fig. 18.

The PD controller output is followed by a saturation block to only output positive pitch angles. The non-zero pitch angle strategy can be adopted by adding a non-zero pitch angle, β_{NZ} to the pitch set point and by expanding the power balancing saturation limit to allow negative angles up to the non-zero pitch value. In addition, the output from the speed control PI controller is saturated to stay above the non-zero pitch value when speed control is enabled.

To prevent excessive switching between the speed control and power balancing control around the nominal operating point, the selector uses hysteresis whereby speed control is activated at nominal rotor speed but only deactivated at 90% rotor speed.

B. Results

Calculating the amount of energy that can be used for balancing using the non-zero pitch operation is not straightforward. The duration the additional power is available is dependent on the rate of change in the wind turbine rotational speed, i.e. how long it takes for the operating point to move from point B to point C. This will depend on the difference between

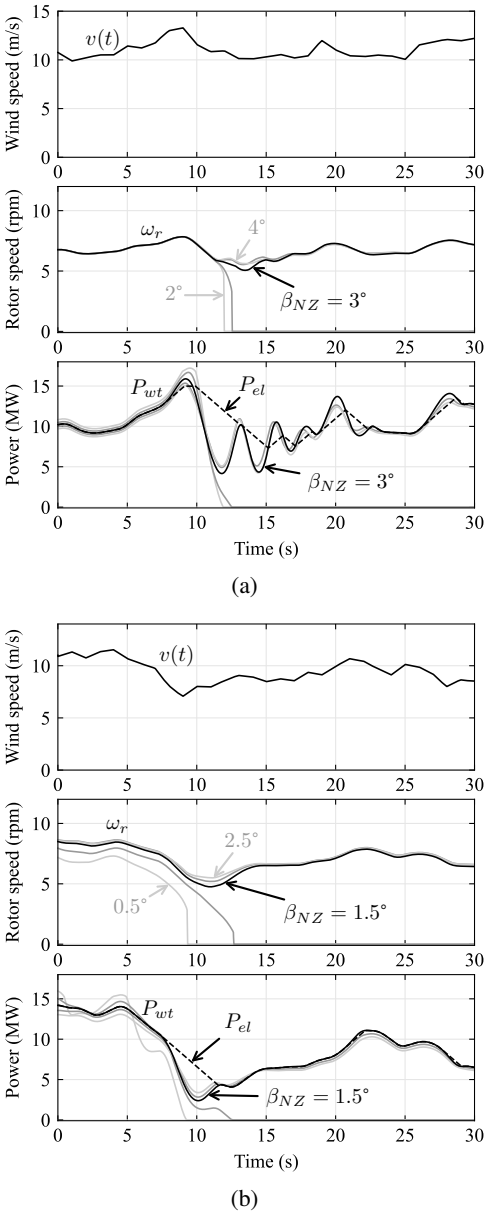

Fig. 19: Time domain results for the non-zero pitch balancing mechanisms, showing the impact of non-zero pitch setting during one of their respective most challenging wind speed reductions, (a) keeping the original tip speed ratio, (b) operating at the new optimal tip speed ratio

the required generator torque and the available aerodynamic torque.

In reality, the tip speed ratio does not remain constant during a wind decrease and will instead increase momentarily. The generator power does not change immediately with a change in wind speed due to the rotor inertia and the blades can also not pitch instantaneously, as the pitch angle rate of change is limited by the pitching actuators. This means the transition between power coefficient curves is not as smooth as Fig. 17 suggests.

To estimate the required non-zero pitch to prevent electrolyzer shutdown, the pitch power balancing algorithm was

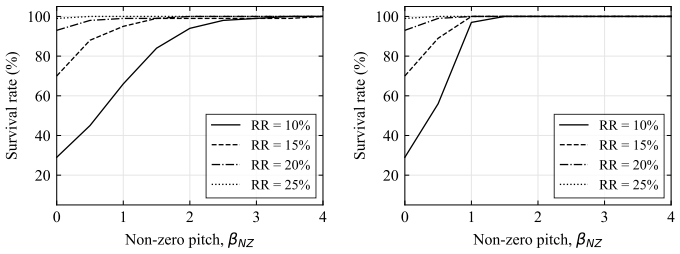

(a) (b)

Fig. 20: Hourly survival rate by non-zero pitch setting, when (a) keeping the original tip speed ratio, (b) operating at the new optimal tip speed ratio

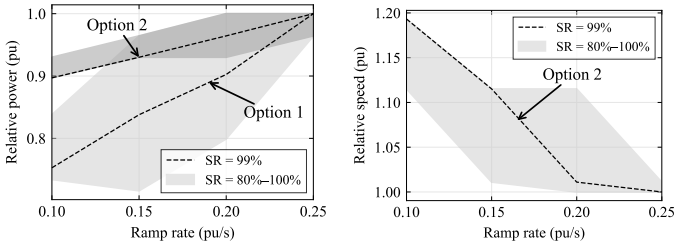

(a) (b)

Fig. 21: Pitch balancing results for varying electrolyzer ramp rates, showing the impact on (a) power production, and (b) rotor speed, by keeping the original tip speed ratio (option 1) or the new optimal tip speed ratio (option 2)

tested on all 100 realistic wind speed scenarios from section IV-B. The pitch angle was adjusted iteratively until the wind turbine could ride through the wind reduction event. In each case, the MPPT torque gain was adjusted to obtain either the original tip speed ratio (option 1) or to obtain the new optimal tip speed ratio at the non-zero pitch angle (option 2). The time domain results for one of the most challenging wind speed reductions for each option are shown in Fig. 19. This shows that option 1 requires a minimum 3° non-zero pitch and option 2 requires a minimum 1.5° non-zero pitch to keep the wind turbine operational through the wind speed event.

The results are shown in Fig. 20 and Fig. 21. For the base case electrolyzer ramp rate of 0.1 pu/s, to enable a 99% survival rate, a non-zero pitch of 3° is required when operating at the original tip speed. This results in a wind turbine power output reduction of 24.7%. By operating the wind turbine at its new optimal speed, a median pitch angle of 1.5° is required, resulting in a power reduction of 10.3% instead. However, this is also associated with a rotational speed increase of 19.3%.

If the electrolyzer ramp rate can be increased, the required non-zero pitch decreases significantly. For example, at a ramp rate of 0.2 pu/s and using option 1, a non-zero pitch angle of 1° is required for a 99% survival rate. This results in a power reduction of 9.8%. When using option 2, the required non-zero pitch angle is 0.5°, corresponding to a power reduction of 3.6%, with a rotational speed increase of 1.1%.

VII. Conclusions

This study investigated the control system for a standalone offshore wind turbine with co-located electrolyzer and how the power between the wind turbine and electrolyzer could be balanced taking into account the electrolyzer ramp rate limitations.

The control system consisted of four main controllers, including the pitch controller, the machine-side converter controller, the line-side converter controller, and electrolyzer-side converter controller. Under normal operation, the machine-side control objective was to maintain the DC-link voltage. The power flow was regulated by the line-side converter control, which employed a grid-forming control structure to generate the electrical angle. The electrolyzer-side converter control objective was to set the electrolyzer voltage to control its power demand.

Three power balancing strategies were investigated, including energy storage, rotor inertia and non-zero pitch. The results showed that for the wind turbine to stay operational through 99% of the hourly wind speed variation while being limited to a 0.1 pu/s power ramp rate, a $6.8M supercapacitor is needed with a rating of 6.7 MW and 8.5 kWh. Alternatively, using rotor inertia to balance the power would reduce energy production by 11% and increase rotor speed by 18%. Using non-zero pitch control would result in a 25% energy reduction without speed increase or a 10% energy reduction with a 19% speed increase. Therefore, at existing commercial electrolyzer ramp rates, none of the balancing strategies are very cost-effective. The most realistic solution would be using energy storage, although this would come at a significant additional capital cost.

Improvements in the power ramp rate of the next generation of electrolyzers would make the production of hydrogen in this system more cost-effective. At higher ramp rates, the control-based power balancing methods become more attractive. For example, at a 0.2 pu/s ramp rate, using rotor inertia balancing results in a power reduction and speed increase of less than 1% and 3%, respectively. For the non-zero pitch balancing strategy with speed increase, these values are 4% and 1%, respectively. These options are therefore both realistic and cost-effective solutions.

If electrolyzer power ramp rates can be increased to 0.3 pu/s, no power balancing or control modifications would be required at all. This should therefore be the design target for future electrolyzers used in off-grid offshore wind systems.

References

[1] S. van Renssen, "The hydrogen solution?," *Nature Climate Change*, vol. 10, no. 9, pp. 799–801, 2020.

[2] B. Parkinson, P. Balcombe, J. Speirs, A. Hawkes, and K. Hellgardt, "Levelized cost of CO_2 mitigation from hydrogen production routes," *Energy & environmental science*, vol. 12, no. 1, pp. 19–40, 2019.

[3] M. Nasser, T. F. Megahed, S. Ookawara, and H. Hassan, "A review of water electrolysis–based systems for hydrogen production using hybrid/solar/wind energy systems," *Environmental Science and Pollution Research*, vol. 29, no. 58, pp. 86994–87018, 2022.

[4] C. Varela, M. Mostafa, and E. Zondervan, "Modeling alkaline water electrolysis for power-to-x applications: A scheduling approach," *International journal of hydrogen energy*, vol. 46, no. 14, pp. 9303–9313, 2021.

[5] O. S. Ibrahim, A. Singlitico, R. Proskovics, S. McDonagh, C. Desmond, and J. D. Murphy, "Dedicated large-scale floating offshore wind to hydrogen: Assessing design variables in proposed typologies," *Renewable and Sustainable Energy Reviews*, vol. 160, p. 112310, 2022.

[6] R. Liu, "The world's first offshore wind power non-desalination of seawater in situ electrolysis for hydrogen production successfully tested in fujian, china," 2023.

[7] M. Müller, K. Litty, and H. Gehritz, "H2Mare update 02/2022," tech. rep., Technology Platform Office, 2022.

[8] International Energy Agency, "The future of hydrogen - seizing today's opportunities," tech. rep., International Energy Agency, 2019.

[9] A. Arsad, M. Hannan, A. Q. Al-Shetwi, M. Hossain, R. Begum, P. J. Ker, F. Salehi, and K. Muttaqi, "Hydrogen electrolyser for sustainable energy production: A bibliometric analysis and future directions," *International Journal of Hydrogen Energy*, vol. 48, no. 13, pp. 4960–4983, 2023.

[10] T. Ayodele and J. Munda, "Potential and economic viability of green hydrogen production by water electrolysis using wind energy resources in south africa," *International Journal of Hydrogen Energy*, vol. 44, no. 33, pp. 17669–17687, 2019.

[11] H. Groenemans, G. Saur, C. Mittelsteadt, J. Lattimer, and H. Xu, "Techno-economic analysis of offshore wind pem water electrolysis for h2 production," *Current Opinion in Chemical Engineering*, vol. 37, p. 100828, 2022.

[12] A. Giampieri, J. Ling-Chin, and A. P. Roskilly, "Techno-economic assessment of offshore wind-to-hydrogen scenarios: A uk case study," *International Journal of Hydrogen Energy*, 2023.

[13] A. G. Dutton, A. J. Ruddell, L. Barra, M. Falchetta, H. Dienhart, W. Seeger, J. A. Bleijs, and A. W. Chung, "Hydrogen generation from stand-alone wind-powered electrolysis systems," Dec 1995.

[14] Siemens Gamesa, "Green hydrogen unlocked: The Brande hydrogen project," 2024. [Online] Available: www.siemensgamesa.com.

[15] Shell, "Shell to start building europe's largest renewable hydrogen plant," 2024. [Online] Available: www.shell.com.

[16] T. Wilberforce, A. Olabi, M. Imran, E. T. Sayed, and M. A. Abdelkareem, "System modelling and performance assessment of green hydrogen production by integrating proton exchange membrane electrolyser with wind turbine," *International Journal of Hydrogen Energy*, vol. 48, no. 32, pp. 12089–12111, 2023.

[17] A. Ursúa, E. L. Barrios, J. Pascual, I. San Martín, and P. Sanchis, "Integration of commercial alkaline water electrolysers with renewable energies: Limitations and improvements," *International Journal of Hydrogen Energy*, vol. 41, no. 30, pp. 12852–12861, 2016.

[18] C. Dixon, S. Reynolds, and D. Rodley, "Micro/small wind turbine power control for electrolysis applications," *Renewable Energy*, vol. 87, pp. 182–192, 2016.

[19] A. E. Samani, A. D'Amicis, J. D. De Kooning, D. Bozalakov, P. Silva, and L. Vandevelde, "Grid balancing with a large-scale electrolyser providing primary reserve," *IET Renewable Power Generation*, vol. 14, no. 16, pp. 3070–3078, 2020.

[20] S. D. Tavakoli, M. G. Dozein, V. A. Lacerda, M. C. Mañe, E. Prieto-Araujo, P. Mancarella, and O. Gomis-Bellmunt, "Grid-forming services from hydrogen electrolyzers," *IEEE Transactions on Sustainable Energy*, 2023.

[21] Á. Hernández-Gómez, V. Ramirez, D. Guilbert, and B. Saldivar, "Development of an adaptive static-dynamic electrical model based on input electrical energy for pem water electrolysis," *International Journal of Hydrogen Energy*, vol. 45, no. 38, pp. 18817–18830, 2020.

[22] J. Gu, B. Guo, S. Hu, S. Ding, T. Zhang, Z. Tian, F. Yang, and M. Ouyang, "Experimental studies on dynamic performance of 250-kw alkaline electrolytic system," *Journal of Power Sources*, vol. 592, p. 233920, 2024.

[23] Y. Zheng, C. Huang, J. Tan, S. You, Y. Zong, and C. Træholt, "Off-grid wind/hydrogen systems with multi-electrolyzers: Optimized operational strategies," *Energy Conversion and Management*, vol. 295, p. 117622, 2023.

[24] B. W. Tuinema, E. Adabi, P. K. Ayivor, V. García Suárez, L. Liu, A. Perilla, Z. Ahmad, J. L. Rueda Torres, M. A. van der Meijden, and P. Palensky, "Modelling of large-sized electrolysers for real-time simulation and study of the possibility of frequency support by electrolysers," *IET Generation, Transmission & Distribution*, vol. 14, no. 10, pp. 1985–1992, 2020.

[25] Siemens Energy, *Silyzer 300 Factsheet*, April 2023. [Online] Available: www.siemens-energy.com.

[26] T. Runser, S. Arend, and R. De Doncker, "Stand-alone offshorewind energy andwater electrolysis: A study on optimal electrolyzer sizing," in *2023 25th European Conference on Power Electronics and Applications*, pp. 1–9, IEEE Power Electronics Society, 2023.

[27] A. Rolan, A. Luna, G. Vazquez, D. Aguilar, and G. Azevedo, "Modeling of a variable speed wind turbine with a permanent magnet synchronous generator," in *2009 IEEE international symposium on industrial electronics*, pp. 734–739, IEEE, 2009.

[28] A. Junyent-Ferré and O. Gomis-Bellmunt, "Wind turbine generation systems modeling for integration in power systems," in *Handbook Of Renewable Energy Technology*, pp. 53–68, World Scientific, 2011.

[29] J. Licari, *Control of a variable speed wind turbine*. PhD thesis, Cardiff University, 2013.

[30] F. D. Bianchi, H. De Battista, and R. J. Mantz, *Wind turbine control systems: principles, modelling and gain scheduling design*, vol. 19. Springer, 2007.

[31] O. Alizadeh and A. Yazdani, "A strategy for real power control in a direct-drive pmsg-based wind energy conversion system," *IEEE transactions on Power Delivery*, vol. 28, no. 3, pp. 1297–1305, 2013.

[32] A. Junyent Ferré, *Control of power electronic converters for the operation of wind generation*. PhD thesis, Universitat Politècnica de Catalunya, 2011.

[33] T.-T. Nguyen, T. Vu, S. Paudyal, F. Blaabjerg, and T. L. Vu, "Grid-forming inverter-based wind turbine generators: Comprehensive review, comparative analysis, and recommendations," *arXiv preprint arXiv:2203.02105*, 2022.

[34] A. Egea-Alvarez, A. Junyent-Ferré, and O. Gomis-Bellmunt, "Active and reactive power control of grid connected distributed generation systems," in *Modeling and Control of Sustainable Power Systems: Towards Smarter and Greener Electric Grids*, pp. 47–81, Springer, 2012.

[35] S. Harrison, *Advancements in converter-based frequency stability: recommendations for industrial applications*. PhD thesis, University of Strathclyde, 2023.

[36] H. Geng, D. Xu, B. Wu, and G. Yang, "Active damping for torsional vibrations in pmsg based wecs," in *2010 Twenty-Fifth Annual IEEE Applied Power Electronics Conference and Exposition (APEC)*, pp. 2126–2131, IEEE, 2010.

[37] A. M. Abomazid, N. A. El-Taweel, and H. E. Farag, "Novel analytical approach for parameters identification of pem electrolyzer," *IEEE Transactions on Industrial Informatics*, vol. 18, no. 9, pp. 5870–5881, 2021.

[38] C. Nichita, D. Luca, B. Dakyo, and E. Ceanga, "Large band simulation of the wind speed for real time wind turbine simulators," *IEEE Transactions on energy conversion*, vol. 17, no. 4, pp. 523–529, 2002.

[39] I. Van der Hoven, "Power spectrum of horizontal wind speed in the frequency range from 0.0007 to 900 cycles per hour," *Journal of Atmospheric Sciences*, vol. 14, no. 2, pp. 160–164, 1957.

[40] K. Mongird, V. Fotedar, V. Viswanathan, V. Koritarov, P. Balducci, B. Hadjerioua, and J.Alam, "Energy storage technology and cost characterization report," tech. rep., Pacific Northwest National Laboratory, 2019.

[41] V. Timmers, A. Egea-Àlvarez, A. Gkountaras, R. Li, and L. Xu, "All-DC offshore wind farms: When are they more cost-effective than AC designs?," *IET Renewable Power Generation*, vol. 17, no. 10, pp. 2458–2470, 2023.